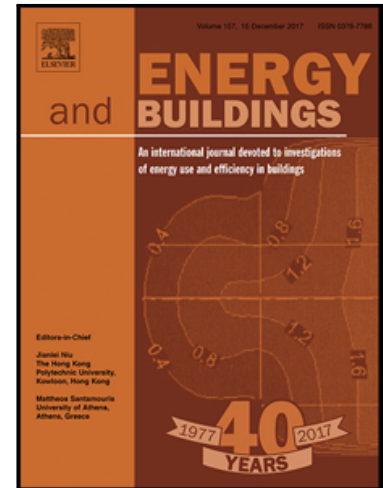


Accepted Manuscript

Simulation and Performance Analysis of an Active PCM-Heat Exchanger Intended for Building Operation Optimization

Navid Morovat , Andreas K Athienitis , José A. Candanedo , Vasken Dermardiros

PII: S0378-7788(19)30578-X
DOI: <https://doi.org/10.1016/j.enbuild.2019.06.022>
Reference: ENB 9248



To appear in: *Energy & Buildings*

Received date: 21 February 2019
Revised date: 31 May 2019
Accepted date: 8 June 2019

Please cite this article as: Navid Morovat , Andreas K Athienitis , José A. Candanedo , Vasken Dermardiros , Simulation and Performance Analysis of an Active PCM-Heat Exchanger Intended for Building Operation Optimization, *Energy & Buildings* (2019), doi: <https://doi.org/10.1016/j.enbuild.2019.06.022>

This is a PDF file of an unedited manuscript that has been accepted for publication. As a service to our customers we are providing this early version of the manuscript. The manuscript will undergo copyediting, typesetting, and review of the resulting proof before it is published in its final form. Please note that during the production process errors may be discovered which could affect the content, and all legal disclaimers that apply to the journal pertain.

Simulation and Performance Analysis of an Active PCM-Heat Exchanger

Intended for Building Operation Optimization

Navid Morovat¹, Andreas K Athienitis¹, José A. Candanedo^{1,2*}, Vasken Dermardiros¹

1: Concordia University, Canada; 2: CanmetENERGY, Canada

Montreal, Québec, H3G 1M8, Canada, jose.candanedoibarra@canada.ca

ABSTRACT

This paper presents a simulation study of an active energy storage device intended to enhance building operation. This device –which is designed for installation in the ceiling plenum of an office, a mechanical room or in other convenient locations– consists of an arrangement of several panels of a phase-change material. It may be charged or discharged as required with an air stream passing between the panels, thus operating as a PCM-air heat exchanger (PCM-HX).

The first part of the paper focuses on the design of the PCM-HX. Several design configurations are evaluated; investigated parameters include the PCM-HX dimensions, the number of air channels and airflow rates. The paper also includes an experimental validation of the PCM model. Performance criteria that were considered in the parametric study include the amount of stored heat, the time needed to charge/discharge the PCM storage and the overall energy density of the device.

The second part of the paper evaluates different control strategies aimed at reducing peak demand and the size of HVAC system. The impact on peak load of a linear ramp for the temperature setpoint is investigated: it was found that a two hour linear ramp in temperature setpoint –together with a PCM-HX configuration with six air channels– can reduce the peak heating load by 41% as compared to a benchmark case without the PCM-HX.

Keywords: Active PCM heat exchanger, Energy storage, Performance optimization, Peak load reduction

1. INTRODUCTION

1.1- Background: PCM for enhanced building flexibility

Energy flexibility in buildings and adequate control of this flexibility are two important factors for the design of smart energy system and buildings. Energy flexible buildings have been defined as those with “the ability to manage [their] demand and generation according to local climate conditions, user needs and grid requirements” [1]. In this context, thermal energy storage in building components can be a key contributor to energy flexibility; phase change materials (PCMs) are a promising technology for this purpose [2, 3]. PCMs apply the principle of latent heat thermal energy storage (LHTES), whereby large amounts of energy are absorbed or released at a certain temperature during the phase change transition period (charging and discharging process) on account of the high heat of fusion of the PCM [4].

PCMs have the benefit of facilitating the storage of heat gains (e.g. passive solar gains), as well as heating energy and cooling energy from the HVAC system [5]. In latent heat storage systems, energy charge and discharge normally occur within a narrow temperature range known as the transition zone [6]. By reducing zone temperature fluctuations, PCMs can reduce energy use, improve thermal comfort and reduce and/or shift the electricity peak demand [7-9]. Their integration in multilayer walls and ceilings reduces the effect of external thermal conditions on the thermal state of the building [10, 11]. Given the large variety of available PCM materials with different thermal properties (such as latent heat storage capacities and phase change temperatures) they can be used in multiple applications. However, for direct building integrations, only PCMs having a phase transition close to human comfort temperature can be used.

Most previous research [12-15] has focused on wall-integrated PCM systems. While these implementations do achieve load reductions, these studies show that integrating the PCM in the surface of a room has a detrimental effect on the controllability of the system, a necessary factor for maximum flexibility and peak load reduction.

This paper presents a novel PCM-HX designed for installation in a ceiling plenum. This study explores the use of an active PCM-HX along with appropriate control strategies as an effective path to optimize the operation of a heating system. Such a dedicated active device offers the advantage of better controllability. At the design stage, considering the energy storage capabilities of a PCM-HX makes it possible to reduce the nominal size of the HVAC equipment required, thus leading to significantly lower initial and operational costs.

1.2- Passive and Active PCM applications

PCM applications can be classified in two main categories: passive systems and active systems, [16]. In *passive* applications, PCMs are integrated into building envelopes to increase the effective thermal storage capacity, thus improving temperature regulation [17, 18]. For example, Athienitis et al. [19] studied a test-room with a PCM-impregnated gypsum board with a particular interest in peak load shifting and solar energy utilization. Passive PCM applications can be particularly beneficial in lightweight constructions with low thermal inertia [20], since the presence of large temperature fluctuations is a well-known issue in these buildings [21]. This is a common problem in some cold climate regions where buildings are built with wood frame construction and large amounts of insulation. In a passive PCM installation, the PCM will typically melt during the daytime to store heat gains (solar and otherwise). During the nighttime, the material will then solidify gradually thus releasing heat to the space. This process will reduce

room overheating during the daytime during the warm months and may decrease the need for space heating during the nighttime in the winter [15, 22, 23].

Active thermal energy storage systems employ a PCM within a stand-alone container or device, which can be melted or solidified as required by using an external heating or cooling source. Active PCM systems provide the following advantages:

- **Flexibility in heat transfer area.** The heat transfer area can be increased by adjusting the ratio of the surface area to the volume of the PCM and airflow rate.
- **Steady conditions for charging/discharging energy.** The high energy density of PCM and the fact that the latent heat transfer process is approximately isothermal result in smaller temperature variations. Active thermal energy storage allows charging/discharging even when indoor conditions are steady, thus facilitating the control of thermal energy.
- **Adjustment of the melting point of the PCM.** In an active installation, it is easier to adjust the melting point (for example, by using a different material). Therefore, the range of conditions that are useful for charging/discharging the PCM can be extended.
- **Integration with mechanical systems.** With mechanical ventilation, enough airflow can be provided to achieve the desired amount of energy storage, peak demand reduction, and load shifting. This peak demand reduction also allows for smaller heating and cooling equipment and ducts, thus saving valuable space in buildings as well as capital cost.
- **Applications in retrofit projects.** Active installations are suitable for retrofits in buildings with low thermal mass since they can add significant controllable and “dispatchable” thermal energy storage.

Mosaffa et al. [24] described an active PCM system intended for free cooling. This device consisted of panels separated by air gaps which enabled air to flow through the PCM. The present study investigates a similar, but not identical, system, designed to control the thermal load of an office space.

1.3- Overview of the paper

The first part of this paper investigates different design options for the integration of active PCM-HX, focusing on the optimization of the storage capacity and controllability. Several parameters are investigated towards achieving an optimal compromise between stored heat and a reasonable time needed to charge/discharge the PCM storage. These parameters include the dimensions of the heat exchanger, the number of air channels and the airflow rate used to charge and discharge the PCM. The mathematical model used in this study for the specific heat of the PCM was validated experimentally; these results are also presented.

In the second part of the paper, the integration of the aforementioned PCM-HX in an office zone is evaluated from the perspective of peak load reduction. This part examines the effect of using a linear ramp of room temperature setpoint transition on peak load reduction. Proportional-integral control (PI) is assumed in the local-loop control of room air temperature. The potential of combining diverse setpoint profiles with PCM designs with different number of air channels is also investigated.

2. ACTIVE PCM-HX: GENERAL CONCEPT

2.1- Geometry of thermal zone

The test building is 4.0 m wide, 4.0 m long and 3.2 m high, without internal partitions. The building, which is of lightweight construction, has a double glazing window in the middle of its

south-facing façade (40% window-to-wall ratio (WWR)). The U-value of the window is $1.2 \text{ W}/(\text{m}^2\text{K})$ and its transmittance is 0.8. Further details on the window properties can be found in a previous study [25]. The bottom opaque section of the facade is 0.8 m high, matching the height of a typical work plane (Figure 1).

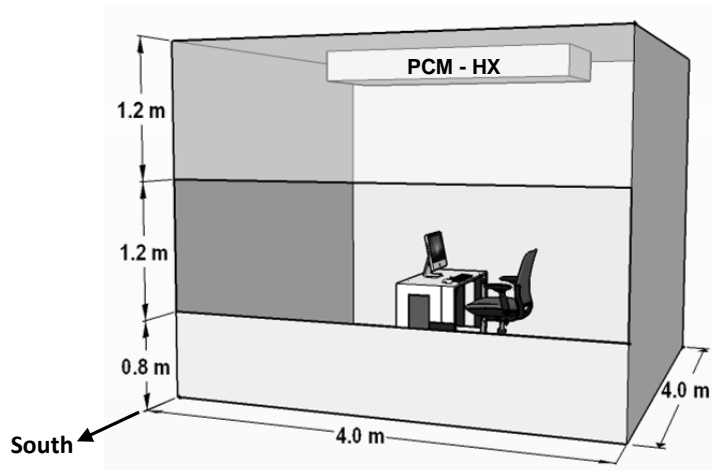


Figure 1. Schematic of the office zone with PCM-HX

2.2- General concept

The present study considers the integration of an actively charged PCM-HX for an office zone, as shown in Figures 2a and 2b. The PCM-HX system (located in this case in a ceiling plenum) is part of an insulated HVAC duct system. An air-handling unit (AHU) with an electric coil, located just before the PCM-HX, is used to preheat the air entering the plenum. A circulation fan is used to drive air between the channels in order to charge/discharge the PCM.

During off-peak hours, hot air from the AHU is used to charge the PCM-HX. If the room requires heating during on-peak hours: (a) the fan is turned on and (b) dampers between the room and the plenum are opened in order to discharge the PCM. The circulation fan can only be either ON or OFF (in other words, no operation at partial flowrates). If required, an electric baseboard heater can provide auxiliary heating directly to the room.

This PCM-HX configuration, which may be used as a practical retrofit measure, opens up the possibility of operating a lightweight building almost like a high-mass building, thus benefiting from the advantages commonly associated with materials with large thermal capacity (e.g., concrete).

The PCM-HX has the following modes of operation:

- **Charging mode:** both the AHU and the fan are turned on to charge the PCM (Figure 2a). The airflow passes through the PCM-HX, and is then recirculated back to the AHU. In this mode of operation, dampers are closed and there is no exchange between the plenum and the room air.
- **Discharging mode:** the AHU is turned off (no heating or cooling provided), but the circulation fan is turned on to discharge the PCM (Figure 2b). This mode of operation opens the dampers that connect the plenum to the room air. Therefore, the discharge mode enables full air exchange with the room during peak load hours.
- **Standby mode:** both the fan and the AHU are off and the dampers are closed. In this mode of operation, there is no exchange between the plenum and the room air.

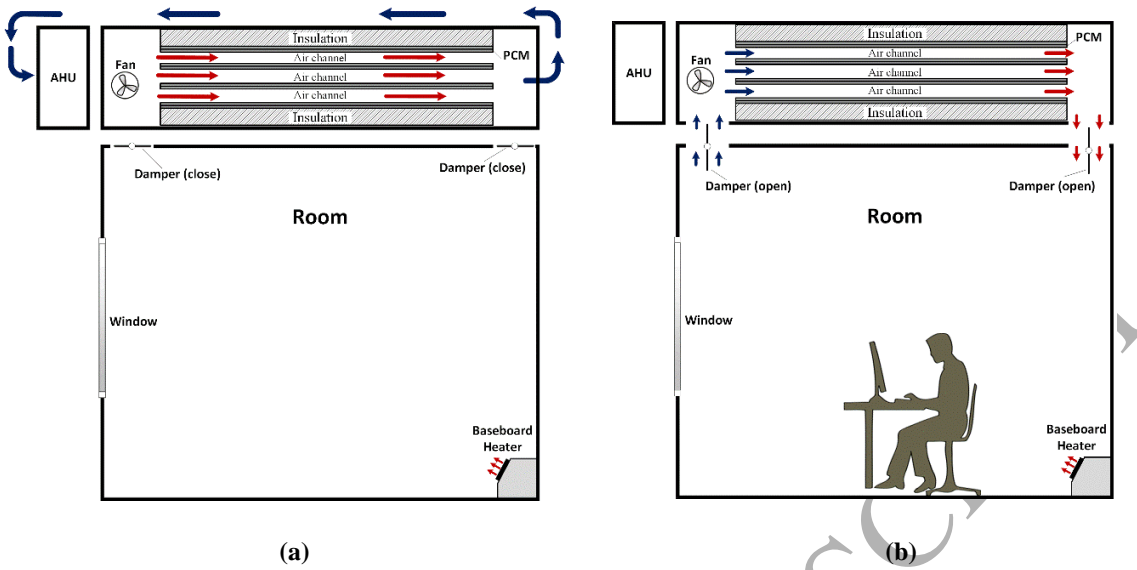


Figure 2. PCM-HX in isolated ceiling plenum (note: drawing not at scale).
 (a) Charging mode (typically at night); (b) Discharging mode (typically in daytime)

Such a configuration, first described in an earlier study [25], provides more flexibility and controllability in terms of charging and discharging temperatures when compared to a conventional wall-integrated PCM system.

2.3- Configuration of PCM-air heat exchanger (PCM-HX)

Figure 3 presents a schematic of the proposed PCM-HX. This device consists of an arrangement of PCM panels that allow an airflow to pass between them. The length, width and thickness of each PCM panel are denoted by L_{PCM} , W_{PCM} and t_{PCM} respectively (standard measures given by the manufacturer for the PCM sheets are $L_{PCM} = 1.2$ m, $W_{PCM} = 1.0$ m and $t_{PCM} = 5.2$ mm). Several PCM panels may be installed “in series” within the PCM-HX; e.g., if n PCM panels are used then: $L_{HX} = n \times L_{PCM}$. For example, Fig. 3 shows two panels connected in series with a total length which is twice that of a single PCM sheet ($L_{HX} = 2L_{PCM}$). The simplicity of the proposed geometry makes this structure more adaptable to different configurations.

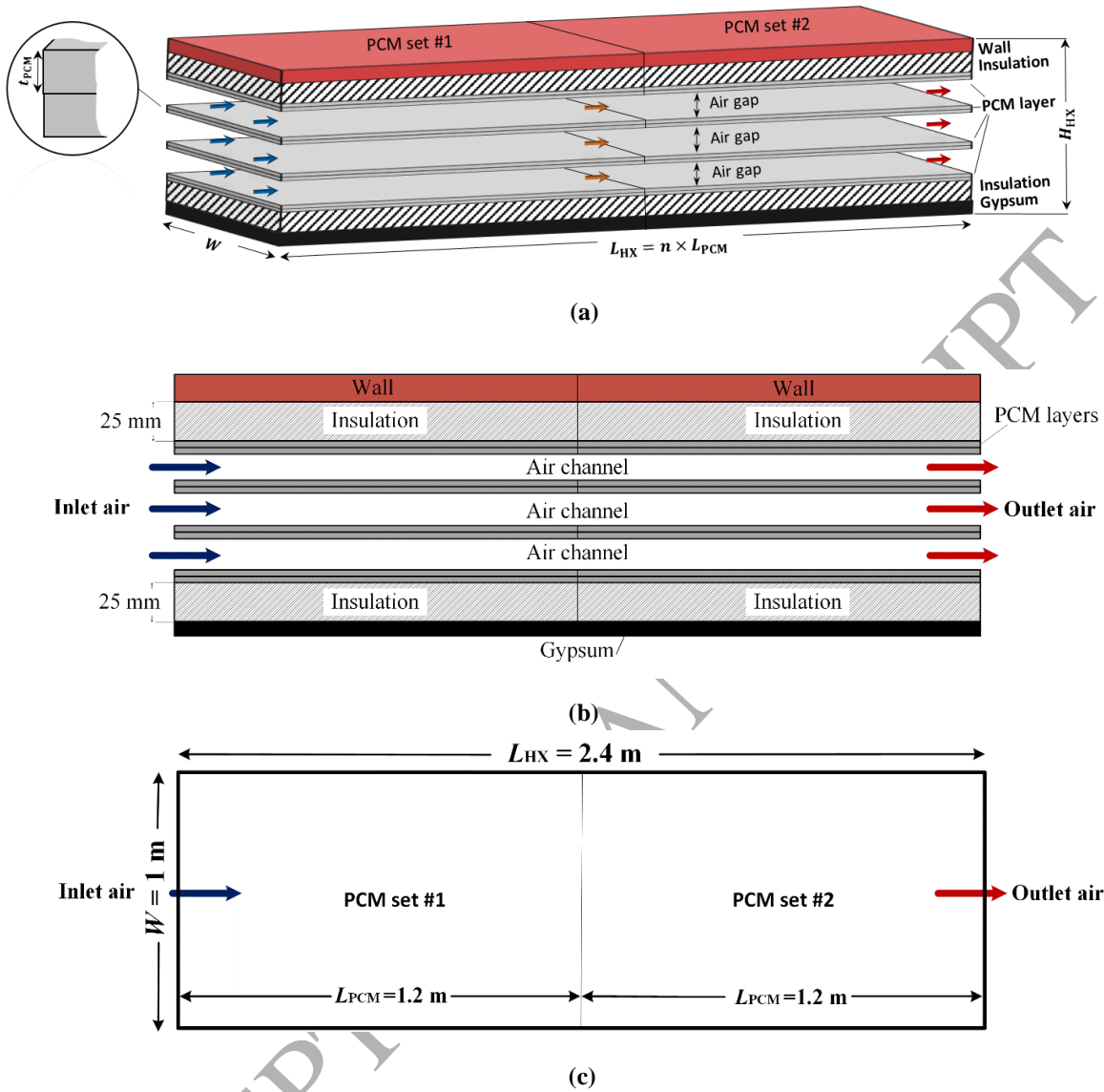


Figure 3. Schematic of PCM-HX. (a) Isometric view, (b) side view, and (c) top view (example with two PCM panels in series)

The PCM used in this paper is DuPont EnergainTM, which consists of a paraffin wax (60 wt. %) embedded in an ethylene-based polymer [13]. Table 1 provides an overview of the thermo-physical properties of the PCM used in the present paper. In a mechanically conditioned space, the best performance is achieved when the PCM melting temperature is around the setpoint temperatures of the room [23, 26, 27]. In this paper, a material with a melting

temperature of 22.3 °C is used. This melting temperature corresponds to typical indoor temperatures in winter; this makes this PCM suitable for heating applications.

Table 1. Properties of PCM used [13]

Element	Quantity
Thickness (base case)	5.2 mm
Density	850 kg/m ³
Average Specific Heat	3500 kJ/kg · K
Peak Melting Temperature	22.3 °C
Latent Heat of Fusion	70000 J/kg
Peak Freezing Temperature	17.8 °C
Conductivity, solid	0.22 W/m · K
Conductivity, liquid	0.18 W/m · K

3. METHODOLOGY

An explicit finite difference scheme, implemented in Python 3.6, is used to numerically solve the heat transfer equations corresponding to the heat transfer phenomena in the office.

3.1- Governing equations – room model

Equation 1 is a finite-difference formulation of the heat balance equation in the office zone.

$$\sum_j [U_{ij}^t (T_j^t - T_i^t)] + \sum_k [U_{ik}^t (T_k^t - T_i^t)] - \frac{C(T)_i}{\Delta t} (T_i^{t+1} - T_i^t) + \dot{Q}_i^t = 0 \quad (1)$$

where

- U_{ij} : Conductance between nodes i and j equal to kA/dx for conductance, $h_{conv}A$ for convection and $h_{rad}A$ for radiation, W/K.
- U_{ik} : Conductance between nodes i and k where node k has a defined or known temperature (boundary condition), W/K.
- $C(T)_i$: Capacitance of node i equal to $k_c \rho C_p(T) A dx$, J/K
- \dot{Q} : Heat flow into the node, W
- Δt : Time step, s.

The capacitance of the air node contains a factor k_C (air capacitance multiplier) that accounts for phenomena (furniture and objects, the time required for air mixing, delay due to ducting and other factors) that in a low-order model result in a capacitance with an observed effective value significantly larger than the one calculated using only the physical properties of the air. In this paper, $k_C = 5$.

The equations in matrix form is:

$$\begin{Bmatrix} T_1 \\ \vdots \\ T_N \end{Bmatrix}^{t+1} = \begin{Bmatrix} \frac{\Delta t}{C_1} \\ \vdots \\ \frac{\Delta t}{C_N} \end{Bmatrix} \odot \left(\begin{bmatrix} -\sum_j^N U_{1j} - \sum_k^M U_{1k} + \frac{C_1}{\Delta t} & U_{12} & \dots & U_{1N} \\ \vdots & \vdots & \ddots & \vdots \\ U_{N1} & U_{N2} & \dots & -\sum_j^N U_{Nj} - \sum_k^M U_{Nk} + \frac{C_N}{\Delta t} \end{bmatrix} \begin{Bmatrix} T_1 \\ \vdots \\ T_N \end{Bmatrix}^t + \begin{Bmatrix} \dot{Q}_1 + \sum_k^M (U_{1kk} T_{kk}) \\ \vdots \\ \dot{Q}_N + \sum_k^M (U_{Nkk} T_{kk}) \end{Bmatrix} \right) \quad (2)$$

where,

- \odot : Is an element-wise multiplication operator,
- N : Is the number of nodes, and,
- M : Is the number of nodes with known temperatures.

A fully explicit finite difference formulation was used to solve the equations. Two heat sources are applied at the room air node: one from the electric heater and the other from an equivalent source from the energy released from the PCM-HX. To assure numerical stability in the solution, the time step must be chosen according to the stability criterion defined in equation 3:

$$\Delta t \leq \frac{\rho \cdot C_p(T) \cdot \Delta x^2}{2k} \quad (3)$$

3.2- Modelling of PCM specific heat

A continuous curve based on a skewed normal distribution requiring five parameters is used (Equation 4) to obtain the effective heat capacity of the PCM as a function of temperature [13]. Hed et al. [28] presented a similar method to simulate a PCM air heat exchanger: they

investigated the effect of different shapes of specific heat curves –as a function of temperature– on the power of a PCM heat exchanger. In the present study, an enthalpy-temperature function for the PCM accounts for enthalpy changes during the phase change. This function is used to estimate an equivalent specific heat at each time step, which is then used in the finite difference equations for PCM. The curve is applicable to PCMs with limited sub-cooling, such as organic materials [29]; it offers a simplified method to incorporate characterization data and improves simulation time.

$$C_p(T) = \Delta h_{PCM} \cdot \frac{1}{\sqrt{2\pi}} \cdot \exp\left(\frac{-(T - T_c)^2}{2 \cdot \omega^2}\right) \cdot \left[1 + \operatorname{erf}\left(\frac{\operatorname{skew} \cdot (T - T_c)}{\sqrt{2} \cdot \omega}\right)\right] + C_{p,\text{average}} \quad (4)$$

where

- h_{PCM} , enthalpy of fusion, kJ/kg ;
- T_c , approximate temperature of peak phase change, $^{\circ}\text{C}$;
- ω , temperature range of phase change, $^{\circ}\text{C}$;
- skew , skewness factor, $^{\circ}\text{C}$;
- $C_{p,\text{average}}$, average, average specific heat of PCM in the sensible range, $\text{kJ/kg} \cdot \text{K}$;

Table 2 presents the specific heat equation parameters used [13].

Table 2. Specific heat equation values for the PCM [30]

Parameters	Melting	Freezing
$\Delta h_{PCM}, \text{kJ/kg}$	13100	12600
$T_c, ^{\circ}\text{C}$	23.6	20.8
$\omega, ^{\circ}\text{C}$	4.5	4.7
Skew, $^{\circ}\text{C}$	-10	-4
$C_{p,\text{average}}, \text{kJ/kg} \cdot \text{K}$	3500	3500

Equation 5 corresponds to the air control volume differential equation.

$$\dot{m} \cdot C_p \cdot dT_{\text{air}} = \text{depth} \cdot dy \cdot (h_{\text{conv.front}} \cdot (T_{\text{front}} - T_{\text{air}}) + h_{\text{conv.back}} \cdot (T_{\text{back}} - T_{\text{air}})) \quad (5)$$

Equation 6 is used to find the outlet air temperature of the control volume. In turn, this information is used to calculate the equivalent heat source at the air channel control volume (Equation 7).

$$T_{\text{air,outlet}} = T_{\text{air,inlet}} \cdot \exp\left(\frac{-h_{\text{conv}} \cdot A_{\text{PCM}}}{\dot{m}_{\text{air}} \cdot C_{\text{p,air}}}\right) + T_{\text{surface}} \left[1 - \exp\left(\frac{-h_{\text{conv}} \cdot A_{\text{PCM}}}{\dot{m}_{\text{air}} \cdot C_{\text{p,air}}}\right)\right] \quad (6)$$

$$\dot{Q}_{\text{PCM}}^t = \dot{m}_{\text{air}} \cdot C_{\text{p,air}} \cdot (T_{\text{air,outlet}}^t - T_{\text{air,inlet}}^t) \quad (7)$$

3.4- Local PI controller

Equation 8 calculates the heat provided by the baseboard heater with proportional-integral control (PI controller) at each time step.

$$\dot{Q}_{\text{heater}}^t = k_p \cdot (T_{\text{setpoint}}^t - T_{\text{room,air}}^t) + k_i \int (T_{\text{setpoint}}^t - T_{\text{room,air}}^t) dt \quad (8)$$

where:

- k_p , proportional gain of the controller, W/K
- k_i , Integral gain of the controller, W/(K · s)

3.5- Convection heat transfer coefficient

The convective heat transfer coefficient within the air channel depends on diverse factors: geometry, airflow rate, fluid and surface temperatures, etc. [28]. Experimental results show that the corrected Martinelli equation (Eq.9) is appropriate for studying active thermal energy storage system with phase change materials with airflow in a cavity [31].

$$\text{Nu}_{\text{Martinelli}} = \frac{\text{RePr} \sqrt{f/2}}{\left(\frac{T_w - T_b}{T_w - T_p} \cdot 5 \cdot (\text{Pr} + \ln(1 + 5\text{Pr})) + 0.5 N_{\text{DR}} \ln\left(\frac{\text{Re}}{60} \sqrt{\frac{f}{2}}\right) \right)} \quad (9)$$

$$h_{\text{conv}} = \frac{\text{Nu} \cdot k_{\text{air}}}{L} \quad (10)$$

3.6- Experimental setup used for validation

The experiments were conducted at the Paul Fazio Solar Simulator Environmental Chamber (SSEC) Research Laboratory (Concordia University, Montréal [13]). This experimental facility allows accurate and repeatable testing of advanced building enclosures under a wide range of conditions with fully programmable temperature, humidity, and pressurization. The temperature inside the SSEC can change in a range from -40°C to $+50^{\circ}\text{C}$. The experiment is used to validate the numerical model of the PCM-HX with one air channel. The experimental test room has 5 layers of PCM panels integrated into the interior surface of the back wall of the room located inside the Environmental Chamber. There is a 30 mm air channel between the 2nd and 3rd layers of the PCM. This PCM integration for thermal storage will be denominated here as the PCM-TES.

Figure 4 shows the experimental setup including the Environmental Chamber and the test room with the wall-integrated PCM. The test room is 3 m wide, 1.5 m long, and 2.7 m high. A circulation fan is used to provide an air speed of around 2 m/s through the air channel. A small auxiliary baseboard heater with a capacity of about 1 kW is used to provide heat into the test room. The PCM used in this experiment has the same thermo-physical properties of the one used in the simulation. Thermo-physical properties of the PCM is presented in Table 1 [30].

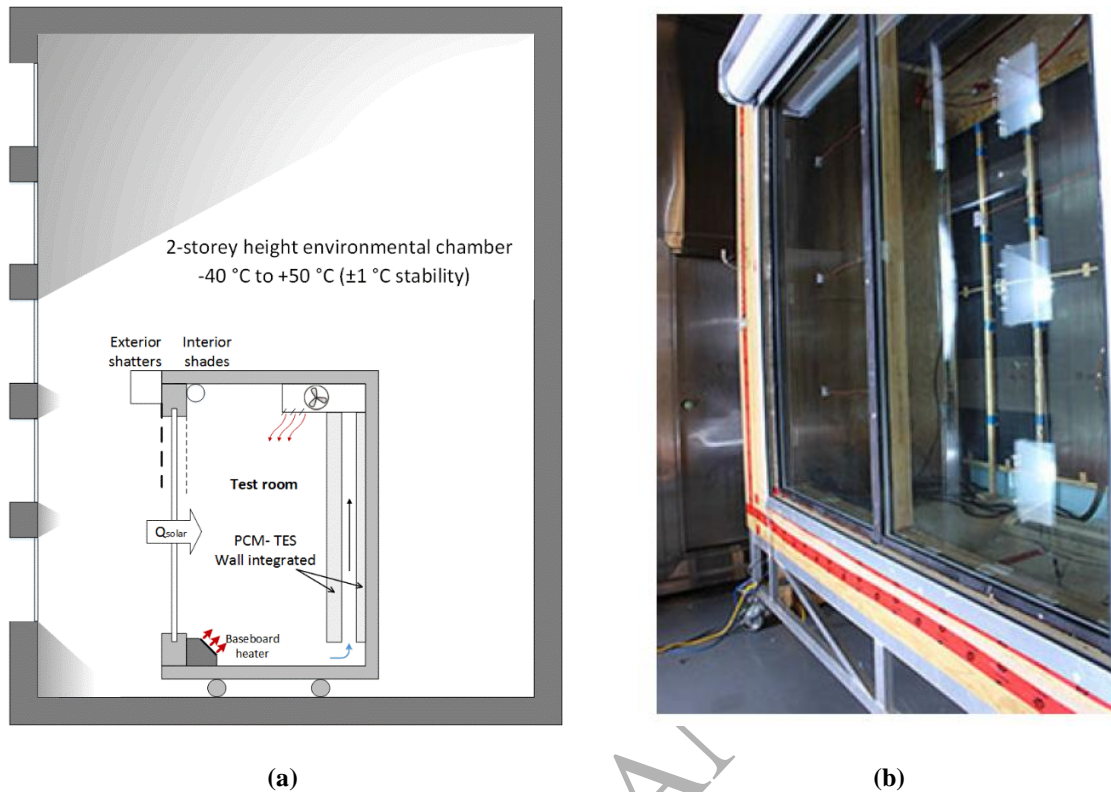


Figure 4. (a) Schematic of the environmental chamber with wall integrated PCM test room. Adapted from Dermardiros [13]. (b) Experimental setup of the test room in the chamber. The front surface of the PCM wall is painted black[13]

Type T thermocouples ($\pm 0.5\text{ }^{\circ}\text{C}$) are used to measure temperatures within the PCM-TES. The Environmental Chamber provides warm/cool air through the PCM-TES. To charge the PCM, hot air stream enters by an inlet plenum of the PCM-TES and exits through an outlet plenum (Figure 5). The inlet and outlet plenum are installed in the test room to assure uniform airflow. At the beginning of the experiment, the PCM-TES is charged by supplying $28\text{ }^{\circ}\text{C}$ air at a rate of 400 kg/s (1.3 m/s average speed) until steady state is attained. This process is run twice to verify repeatability. The flow rate was chosen since it would provide a good convection heat transfer rate with lower pressure losses. The temperatures are read every 30 seconds and the average is recorded every minute. The experiments investigated the charge/discharge rate of the PCM under a temperature range of $16\text{ }^{\circ}\text{C}$ to $25\text{ }^{\circ}\text{C}$ in the test room. Further details of the experimental setup is

presented by Dermardiros [13].

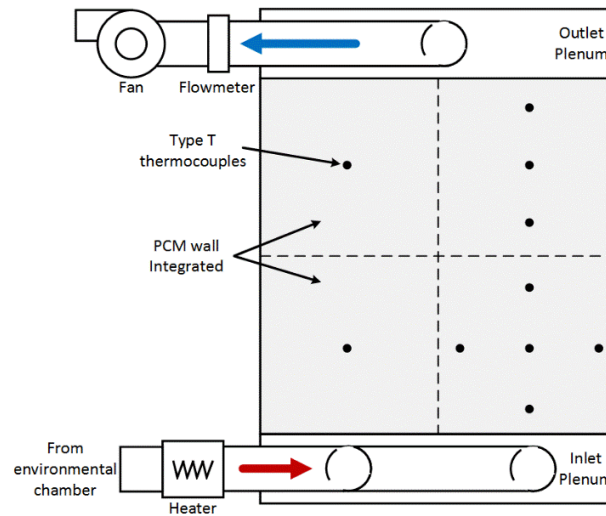


Figure 5. Schematic of the PCM wall integrated experiment. Adapted from Dermardiros [13]

3.7- Experimental validation of the numerical simulation

The current study shows how an explicit finite difference method with an enthalpy-temperature function for the PCM can be used as an effective tool in the design and implementation of the rule based control strategies in a test room with PCM-HX. Figure 6 and 7, presents a comparison between results of the numerical simulation and corresponding experimental data [13], and their coefficient of variation of the root mean square error (CV-RSME). In this regard, the air outlet temperature (Figure 4) and energy transferred by the PCM-HX (Figure 5) is investigated. It was found that the PCM model can accurately predict the energy transferred by the PCM and the room temperature profile ($CV-RSME \leq 5\%$). While this experimental configuration is different from the proposed PCM-HX device, these results illustrate the validity of the PCM enthalpy model.

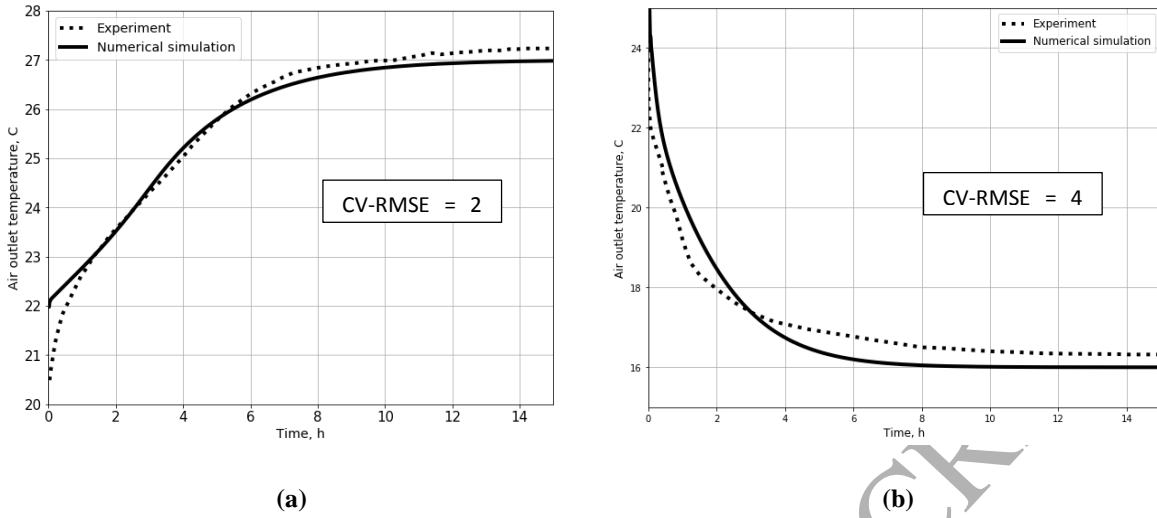


Figure 6. Numerical simulation and experiment results for air outlet temperature:
(a) Charging mode, (b) Discharging mode

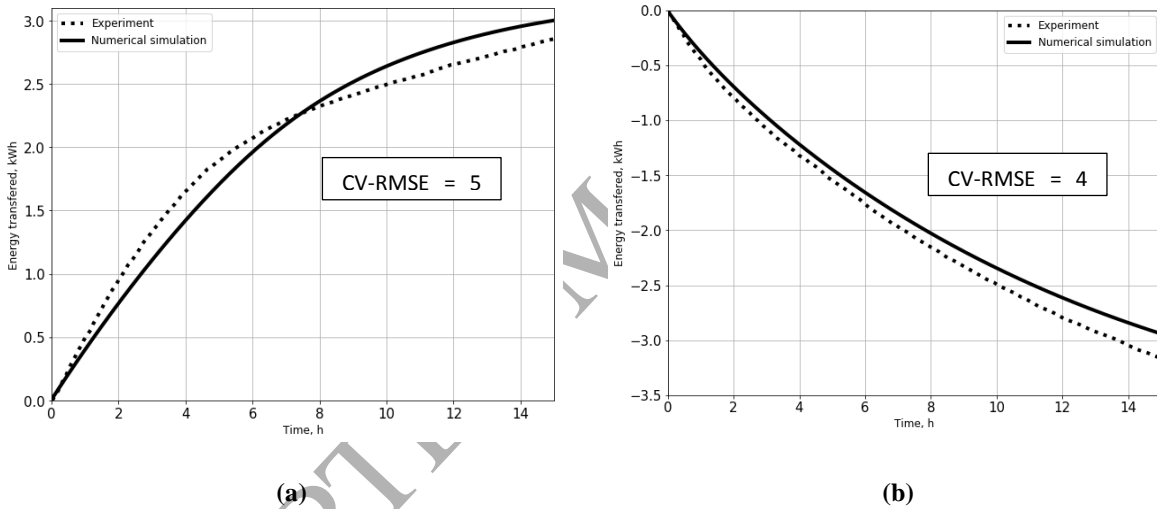


Figure 7. Numerical simulation and experiment results for energy transferred of the PCM-HX:
(a) Charging mode, (b) Discharging mode

4. PARAMETRIC DESIGN ANALYSIS

Results of this paper are presented in two parts:

- (a) Evaluation of the design parameters, which include PCM thickness (t_{PCM}), PCM-HX length (L_{PCM}), airflow rate through the channels, and the number of air channels. One parameter was fixed: the number of PCM layers, which was kept constant at eight (8).
- (b) Application of the PCM-HX integrated into the office zone under different control strategies.

4.1- Parameters investigated

The PCM-HX system is studied by varying the dimensions of the PCM and air channel, with different lengths (1.2, 2.4 and 3.6 m, corresponding to 1, 2 or 3 PCM panels in series). The inlet airflow rate was varied between 200 kg/h and 500 kg/h. Turbulent flow regime in the air domain was assumed ($3060 < Re < 7650$). Table 3 provides an overview of the values of all parameters investigated in this study.

Table 3. List of varied parameters

Case	Mass flow rate (kg/h)	Volume flow rate (L/s)	Average velocity (m/s)	PCM layer thickness (mm)	Air channel height (mm)	PCM-HX length (m)	Re number	Internal Convection Coefficient ($W/m^2 \cdot K$)
Effect of airflow	200	47.48	1.56	5.20	30.00	1.20	3060.00	9.62
	300	71.22	2.34	5.20	30.00	1.20	4590.00	15.32
	400	94.96	3.12	5.20	30.00	1.20	6120.00	20.50
	500	118.70	3.91	5.20	30.00	1.20	7650.00	26.62
Effect of PCM layer thickness	200	47.48	1.56	3.00	30.00	1.20	3060.00	9.62
	200	47.48	1.56	5.20	30.00	1.20	3060.00	9.62
	200	47.48	1.56	7.00	30.00	1.20	3060.00	9.62
	200	47.48	1.56	10.00	30.00	1.20	3060.00	9.62
Effect of PCM-HX length	200	47.48	1.56	5.20	30.00	1.20	3060.00	9.62
	200	47.48	1.56	5.20	30.00	2.40	3060.00	9.62
	200	47.48	1.56	5.20	30.00	3.60	3060.00	9.62
	200	47.48	1.56	5.20	30.00	4.80	3060.00	9.62

Air was assumed to have constant density, thermal conductivity and specific heat, with values of 1.184 kg/m^3 , $0.0255 \text{ W/(m}\cdot\text{K)}$ and $1006 \text{ J/(kg}\cdot\text{K)}$, respectively. For each parametric combination, a numerical experiment was carried out by turning on the fan at time $t = 0$, and making it run for a 24-h period, with a constant inlet temperature of $10 \text{ }^\circ\text{C}$. Simulation results are presented below.

4.2- Effect of airflow through air channels

Airflow rates of 200, 300, 400 and 500 kg/h were investigated for a configuration with one air channel (Figure 8).

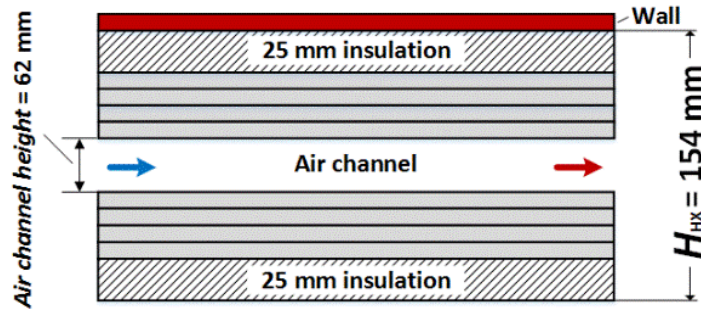


Figure 8. Schematic of PCM-HX with one air channel

Figure 9a and 9b provides the air outlet temperature and power delivered to the airstream by the PCM-HX for the different air flow rates, respectively.

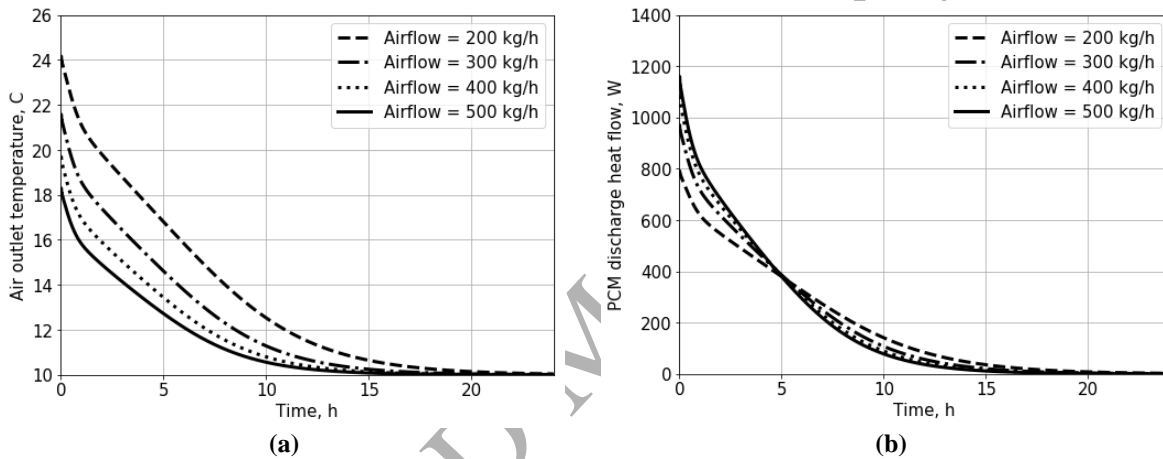


Figure 9. Effect of airflow on : (a) air outlet temperature, (b) PCM-HX power output of the PCM-HX

As expected, the air temperature difference between outlet and inlet decreases as the air flow rate increases. The average ΔT 's are 14 °C, 11 °C, 9 °C and 8 °C for air flow rates of 200, 300, 400 and 500 kg/h respectively.

At the beginning of the numerical experiment, high flow rates provide a higher power output (nearly 1200 W for 500 kg/h, versus 800 for 200 kg/h). However, low airflow rates discharge the PCM-HX more slowly. As a result, the average energy transfer over a 24 h period for the four air flow rates is approximately the same: it amounts to roughly 4.4 kWh. The amount of energy transferred was computed by using Equation 7.

4.3- Effect of the thickness of PCM layers

Another investigated parameter was the thickness of the PCM layers (see Table 3). Simulations were performed to study the effect of the thickness of the PCM sheets in order to find the optimum PCM volume for the integration of the system in an office zone. Simulations were done by testing several PCM-HX systems with PCM layers of various thicknesses (3, 5.2, 7, and 10 mm). Figure 10 presents the air outlet temperature and heating power delivered by the PCM-HX over a 24 h for different thicknesses.

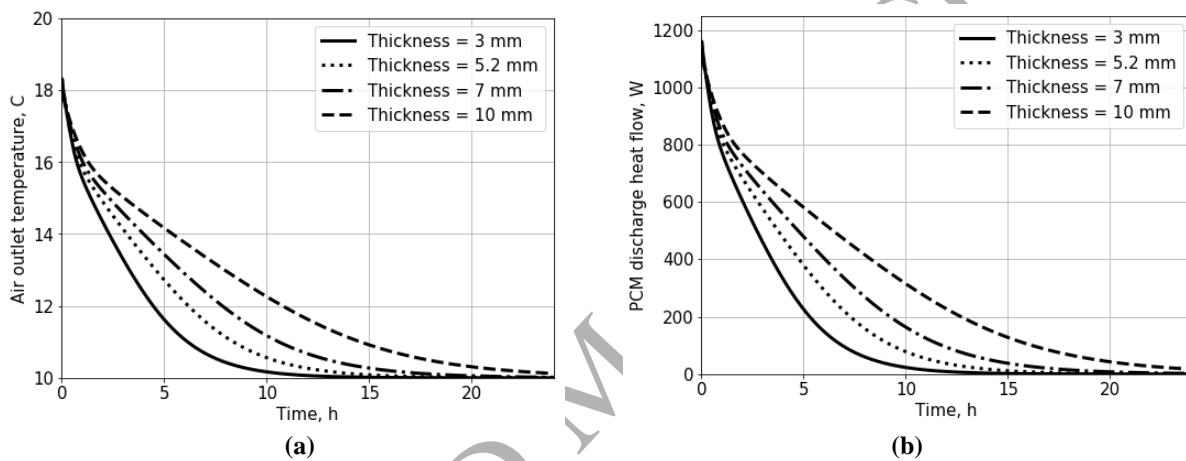


Figure 10. Effect of PCM layer thickness on : (a) air outlet temperature, (b) power output of the PCM-HX

Figure 10 show that the different configurations have a similar temperature decay profile. The slightly different temperature-profile is caused by the thicker volume of PCM layer used. Increasing the thickness of the PCM layers results in higher outlet air temperature and higher PCM-HX output power. Thicker PCM sheets lead to a larger amount of energy stored; conversely, the larger thickness of PCM layer means longer times are needed to discharge them.

4.4- Effect of length of the PCM-HX

In this section, identical 1.20 m systems are placed “in series” (i.e., one after another) to obtain devices with total lengths of 1.20, 2.40, 3.60 or 4.80 m. Figure 11 provide results regarding the effect of length of the PCM-HX on air outlet temperature and PCM-HX power.

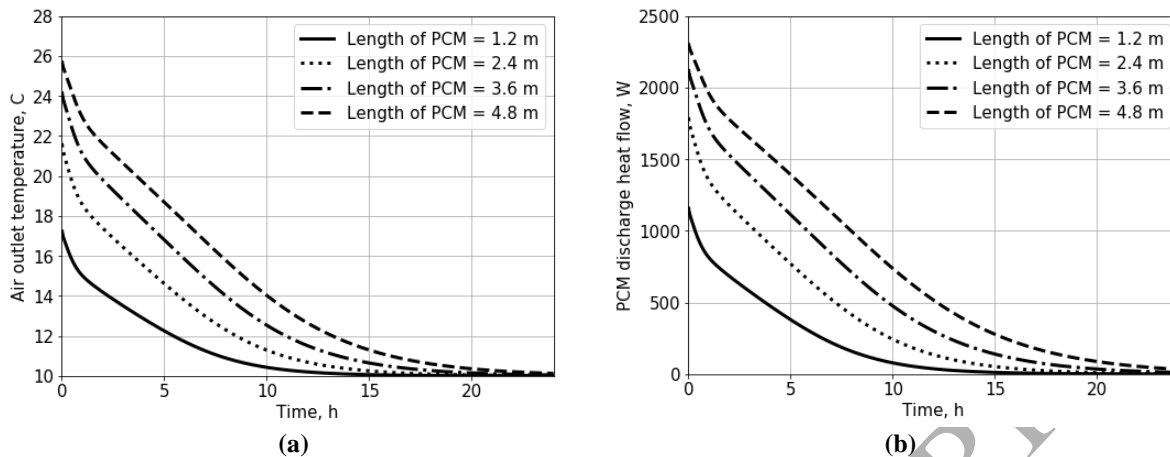


Figure 11. PCM-HX length on: (a) air outlet temperature, (b) power output of the PCM-HX

Increasing the length of the PCM-HX leads to higher power output and also higher air outlet temperature, but more time is required to charge/discharge the system. As expected, the difference between outlet and inlet air temperature increases for longer PCM-HX devices. The difference between outlet and inlet air temperature are 7 °C, 12 °C, 14 °C and 16 °C for PCM-HX lengths equal to 1.2, 2.4, 3.6 and 4.8 m respectively.

Conversely, longer PCM-HX devices imply higher pressure drops through the system, and consequently increasing fan power required. This is another design factor that must be taken into account.

4.5- Effect of the number of air channels

The number of air channels through the PCM layers was also investigated. Figure 12 shows the different configurations of the PCM-HX consists of 8 PCM sheets with 1, 2, 3 or 6 air channels between layers studied in this paper.

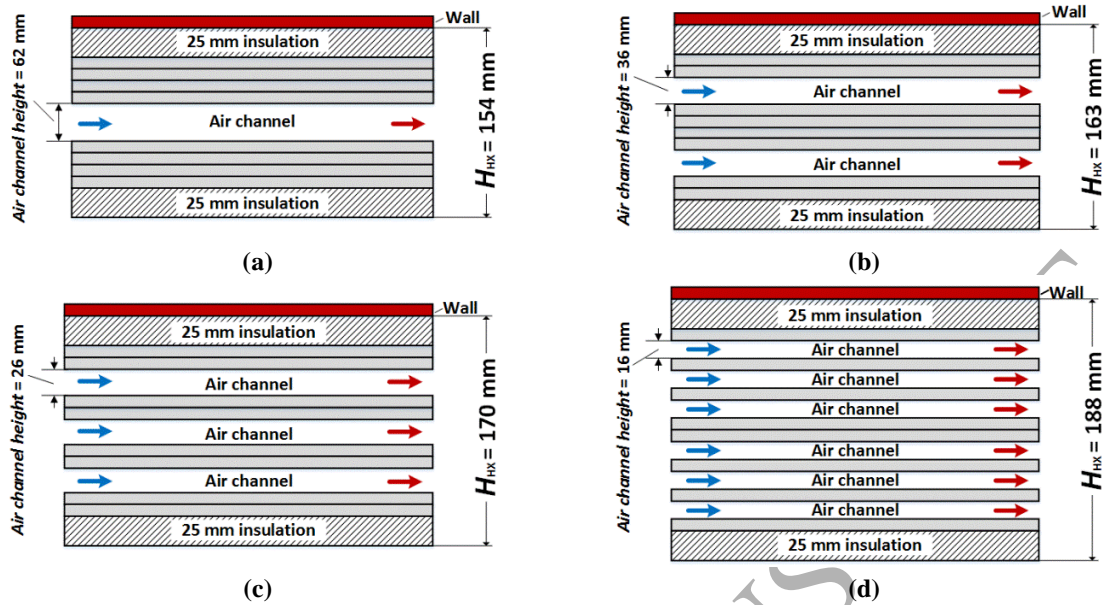


Figure 12. Schematic of PCM-HX with the different number of air channel: (a) one channel; (b) two channels; (c) three channels; (d) six channels.

The total mass flow rate considered is 600 kg/h (turbulent flow through air channels) for all cases with different number of air channels. For comparison purposes, the height of the channels and air velocity were chosen in order to maintain both a constant convective heat transfer coefficient and a constant total mass flow rate across the different systems [31]. Accordingly, the inlet air velocity varies between 1.47 m/s and 2.23 m/s assuming turbulent flow in the air cavity. The smallest Reynolds number is 3040 for the 6-air channel configuration (slowest flow). Table 4 presents the value of the parameters for different numbers of the air channels.

Table 4. List of parameters for different number of air channel [31]

Number of channels	Total mass flow (kg/h)	Volume flow rate (L/s)	Mass flow (kg/(s · channel))	Average velocity (m/s)	Air channel width (mm)	Convection Coefficient (W/m ² · K)	Re number
1	600	142.40	0.17	2.23	62	18	17200
2	600	142.40	0.08	1.93	36	18	8830
3	600	142.40	0.06	1.75	26	18	5830
6	600	142.40	0.03	1.47	16	18	3040

The multi-channel active PCM-HX is analyzed comparatively using the thermal network model described in the section 3. Figure 13a and 13b presents the air outlet temperature of the

PCM-HX, and PCM-HX power in 24 hours period for different number of air channels, respectively.

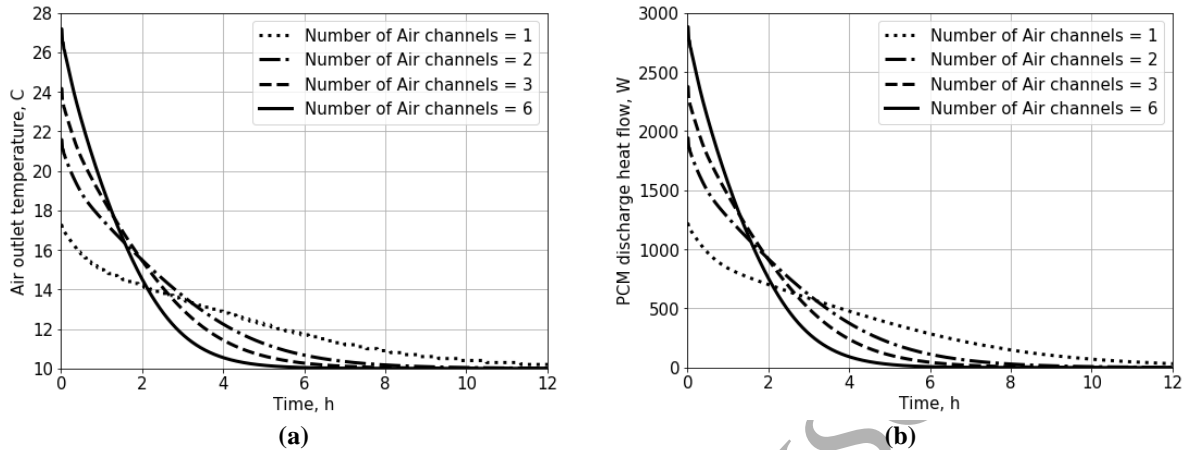


Figure 13. Effect of number of air channels on: (a) air outlet temperature vs. time, (b) power output of the PCM-HX vs. time.

Results show that the charge/discharge time is inversely proportional to the number of channels. The single channel system would take more than 7 hours to discharge, and would not be useful for fast peak reduction measures. In contrast, a 6-channel PCM-HX system provides faster and more easily controllable storage of heat/cool. Table 5 provides a summary of the results regarding energy per unit of volume of the PCM-HX (kWh/m^3), charging and discharging time (h) for different number of air channels.

Table 5. Energy density, charging and discharging time for different number of air channel

Number of channel	Energy per unit of volume of the PCM-HX (kWh/m^3)	Charging time (90%) (hr)	Discharging time (90%) (hr)
1 Channel	67.56	7.25	8.56
2 Channel	61.61	4.30	5.15
3 Channel	58.52	3.40	4.00
6 Channel	50.87	2.58	3.10

Based on the results presented in Table 5, although increasing the number of air channels leads to lower energy density (per unit of volume of the PCM-HX), the charging and discharging times are shorter; in other words, this results in “faster” (and arguably more controllable) PCM-HX devices. Increasing the number of air channels from 1 to 6, reduces the energy per unit of volume by 25% while accelerating the charging and discharging time by 64%.

5. CONTROL STRATEGIES

The appropriate application of control strategies in HVAC systems is a key factor to improve the energy efficiency [25, 32, 33] and energy flexibility of buildings [1, 34, 35]. Advanced control strategies for PCM, including predictive control, have been investigated. For example, Barzin et al. [36] studied the application of weather forecasts to passive solar buildings with PCM; energy savings of about 31% were found.

Thermal energy storage systems with PCM have not been widely adopted, arguably due to the lack of a proper integration into the building HVAC systems. In this regard, proper integration, including suitable control strategies, has a significant impact on the performance of the system. Also, if integrated with HVAC system design, the inclusion of the PCM-HX can be used to avoid the common practice of oversizing the HVAC equipment. Thus, both the operating and capital costs of the system can be reduced in an effective manner.

The results presented so far have discussed the amount of stored heat, the time needed to charge/discharge the PCM-HX and the overall energy density of the device. The integration of the active PCM-HX within the HVAC system for peak load reduction was investigated. The sizing of the PCM-HX to achieve the optimal energy storage, peak demand reduction, and load shifting was investigated. This peak demand reduction may also enable smaller heating and cooling equipment and ducts, with a consequent reduction of equipment size and costs.

The following sections summarize the results obtained from the application of the PCM-HX integrated into an office zone under three different control scenarios. Firstly, the effect of the PCM-HX heat contribution is studied when a step setpoint change is applied. Secondly, the effect of using a linear ramp of room temperature setpoint on reducing peak load (with and

without PCM-HX) is investigated. Finally, the effect of the number of air channels on peak load reduction is discussed.

5.1- Design day conditions for control studies

Weather conditions similar to a winter day in Montreal (i.e., a “Design Day”) are selected as the simulation scenario, since the electrical power demand tends to peak under these conditions. Figure 14 presents the curves used to model outdoor temperature and solar flux on the south facade. In this simulation scenario, it is assumed that the outside temperature follows a perfect sine curve, fluctuating between $-20\text{ }^{\circ}\text{C}$ and $-10\text{ }^{\circ}\text{C}$ (thus having $-15\text{ }^{\circ}\text{C}$ as a mean temperature, with an amplitude of $5\text{ }^{\circ}\text{C}$). The peak temperature is reached at 3 pm. The time-varying solar flux is assumed to have a distribution representing an overcast cold day in February; this curve was obtained from a simulation carried out using EnergyPlus [37] with a Montreal weather file.

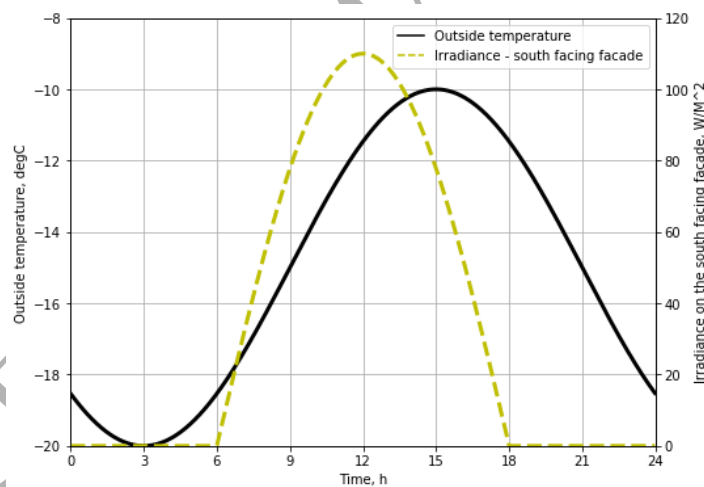


Figure 14. Outdoor temperature and solar flux on the south facade

5.2- Numerical experiment

It was assumed that the PCM-HX was well insulated on all sides (i.e., adiabatic conditions). The initial conditions of the experiment (just before $t = 0$) were the following:

- The initial temperature of the room was set at 18 °C everywhere.
- It was assumed that the PCM-HX was “fully charged”: the material is fully melted and at a uniform temperature of 28 °C.
- Air from the room is circulated through the PCM-HX whenever heat extraction is required.

The simulation starts at $t = 0$ and runs for a period of 24 h using the weather conditions presented in Figure 15. The simulation time step was set to 60 seconds (it was previously determined that the critical time step for the finite difference formulation was 87 s). The heat provided by the baseboard heater was calculated by using a simple proportional-integral control. Proportional gain of the controller (k_p) is assumed to be twice the capacity of the electric baseboard heater per degree (e.g., if the baseboard capacity is 3000 W, $k_p = 6000$ W/K), and the k_i is assumed to be 0.1 W/K·s

5.3- Peak load shifting with PCM-HX

Lowering the temperature setpoint at night is an effective way to reduce energy consumption [38, 39]. In this case, the setpoint during the daytime (between 6:00 to 18:00) is 22°C, and the nighttime (between 18:00 to 6:00) setpoint is 18 °C. The energy released from the PCM-HX is considered as the primary heating system; an electric baseboard provides auxiliary system.

It should be taken into account that oversized systems cycle off before they completely heat or cool a zone. In addition, an undersized system runs constantly trying to heat the zone, but it cannot provide the required thermal comfort. Therefore, having a properly sized HVAC system that matches the demand can provide thermal comfort while reducing peak loads. With this in mind, a baseboard heating system with capacity of 1000 W is used. The charging mode of the PCM-HX device is from 0:00 to 6:00 (off-peak hours) and discharging mode is from 6:00 to

15:00 (on-peak hours). The application of the PCM-HX system toward achieving peak load shifting and peak load shaving has been investigated under these conditions.

Figure 15 shows the set point and room air temperature with and without the PCM-HX. As can be seen, the small baseboard heater without a PCM-HX cannot reach the required setpoint. Conversely, these results show that a PCM-HX manages to keep comfortable indoor conditions, even with a small baseboard. Figure 16 presents a comparison of the results for the electric load (AHU coil + baseboard heater) with and without PCM-HX.

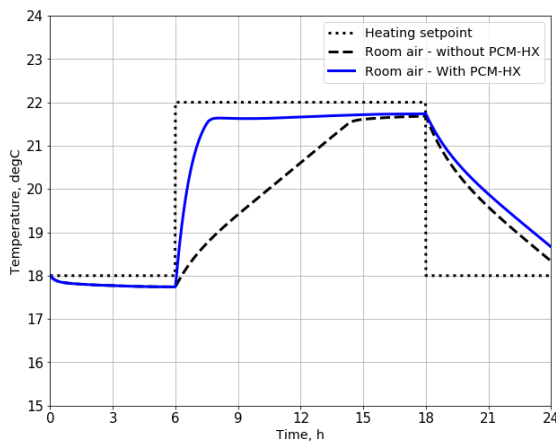


Figure 15. Temperature setpoint and room air temperature

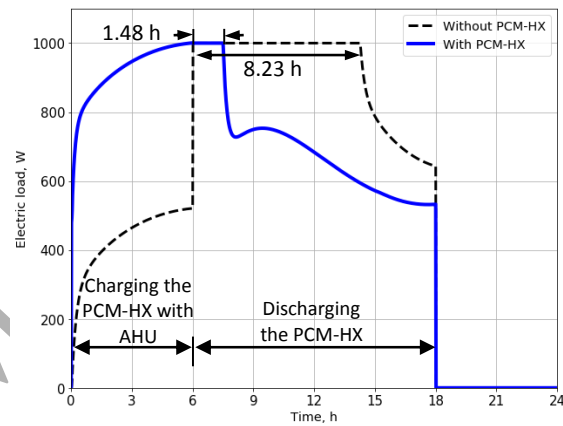


Figure 16. Heating load with and without PCM-HX

These results show that using PCM-HX can reduce peak load duration from 8.23 to 1.48 h. Figure 16 shows that using PCM-HX shifts the peak load from on-peak hours to off peak hours and reduces the peak load *duration* by 82 %, therefore reducing the mean power load during daytime (W) by 31% (from 915 W to 695 W).

5.4- Peak load reduction with PCM-HX and linear ramp of room temperature set point

It is well known that a sudden setpoint transition –e.g. between a night setback and daytime setpoint– creates a spike in the peak demand. The effect of using ramps to transition between setpoints has been investigated by [40-42], among others.

This section examines the effect of using two-hour linear ramp of room temperature set point on reducing peak load in a room equipped to PCM-HX with six air channels. In this case, a baseboard heater with capacity of 3000 W is used for better thermal comfort. The charging mode of the PCM-HX device is from 0:00 to 4:00, and the discharging mode is from 04:00 to 15:00. Figure 17 presents thermostat set point with ramp and room air temperature. Figure 18 presents results regarding heating load required considering ramp in set point temperature with and without PCM-HX.

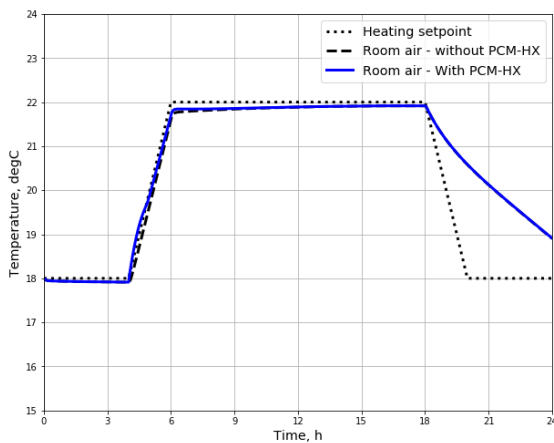


Figure 17. Temperature setpoint with ramp and room air temperature

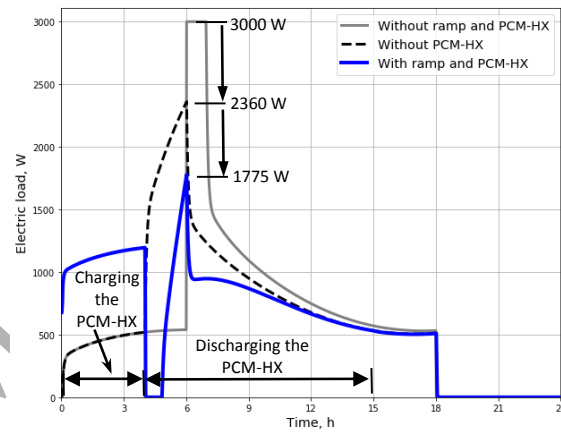


Figure 18. Heating load with and without PCM-HX – set point temperature with ramp

Results presented in Figure 17 show that a 2 hour ramp in temperature set point can reduce peak load by 21% from 3000 W to 2360 W. The combination of the 2 hours linear ramp and a PCM-HX device with six air channels provides 41% peak load reduction (from 3000 W to 1775 W).

5.5 - Energy flexibility

The role of buildings as flexible loads is becoming more important; they can act as energy generators, energy storage, or/and controllers of demand [43]. Energy flexibility in buildings has been defined as “the possibility to deviate the electricity consumption of a building from the reference scenario at a specific point in time and during a certain time span” [44]. Table 6

provides a comparison (in terms of flexibility) between the reference case (without PCM-HX) and the case with PCM-HX and 2 hours linear ramp.

Table 6. Energy Flexibility of the building

Flexibility parameter	Without ramp and PCM-HX	With ramp and PCM-HX	Changes relative to Ref. case
Peak load (W)	3000	1775	41% reduction
Mean power load during daytime (W)	988	775	22 % reduction

The results presented in Table 6 show that such a PCM-HX device together with appropriate control strategies could provide flexibility to the grid, reduce mean power load during daytime and peak power demand, simultaneously.

6. CONCLUSIONS

This study presented in this paper investigated different design options of active PCM-HX charged and discharged with a controlled airflow in an office zone. The paper also includes an experimental validation of the PCM model. It was found that the model of the PCM can accurately predict ($CV-RSME \leq 5\%$) energy transferred and air outlet temperature from the PCM-HX.

In the first part of the paper, the effect of thickness, length, number of the air channels, airflow rates, and energy storage of the PCM-HX were evaluated. Results show that:

- Increasing the length of the PCM-HX leads to higher power output and also greater air-outlet temperature, but longer times are needed to charge/discharge the system.

Results show that, for charging/discharging times of about 8 h (or less), a PCM-HX device with 2.4 m length has a good thermal performance and controllability.

- The difference between the outlet and inlet air temperature decreases with the increase in air stream rate, while the average energy transfers for different airflow rates are approximately the same. Therefore, in turbulence air stream through PCM-HX, lower the airflow rate leads to the better performance of the system (in terms of energy consumption and noise).
- Although increasing the number of air channels in PCM-HX reduces the energy per unit of volume, the charging/discharging time is shorter. This results in faster and more easily controllable PCM-HX. For instance, increasing the number of air channels from 1 to 6 led to a reduction of energy density 25%, but the charging/discharging time was 64% faster.

The PCM-HX presented in this paper is a lightweight solution in buildings with low thermal mass to increase the effective thermal storage capacity of a building as well as increasing controllability of the stored energy.

In the second part of the paper, the integration of the proposed PCM-HX in an office zone is evaluated along with the effect of enhanced control strategies. The potential of using PCM-HX with different numbers of air channels together with linear ramps was investigated. The main results are:

- The combination of a small baseboard heater (1000 W), and a PCM-HX device with six air channels shifts the peak load from on-peak hours to off peak hours and reduces the peak load *duration* by 82 %. It also results in 31% reduction in mean power load during daytime, relative to a reference case without the PCM-HX;
- For a larger baseboard heater (3000 W), the combination of the two-hours linear ramp of temperature setpoint and PCM-HX with six air channels provides 41% peak load

reduction, and 22% reduction in mean power load during daytime, relative to a benchmark case without the PCM-HX;

Results shows that the use of active PCM-HX and appropriate control strategies could be an effective solution to enhance energy flexibility in buildings, reduce the sizing of the HVAC units at the design stage and achieve savings both in initial capital expenses and system operation cost.

ACKNOWLEDGEMENTS

Technical support from Hydro-Quebec Laboratoire des Technologies de l'Énergie Shawinigan research center under NSERC/Hydro-Quebec industrial research chair is greatly acknowledged. The authors would like to thank NSERC for the funding of this project through Dr. Candanedo's Discovery Grant, and the NSERC/Hydro-Québec Industrial Research Chair ("Optimized operation and energy efficiency: towards high performance buildings") held by Dr. Athienitis. The comments of our colleagues at Concordia and Canmet are gratefully appreciated.

NOMENCLATURE

C_{avg}	Average specific heat of PCM in the sensible range ($J/kg \cdot K$)	T	Temperature ($^{\circ}C$)
C_i	Thermal capacitance of node i (J/K)	T_{sp}	Room air setpoint ($^{\circ}C$)
C_p	specific heat ($J/kg \cdot K$)		Greek letters
h_{conv}	Heat conduction coefficient ($W/m^2 \cdot K$)	ρ	Density (kg/m^3)
k	Heat conduction coefficient ($W/m \cdot K$)	ω	Temperature range of phase change
k_C	Air capacitance multiplier (-)		
k_p	Proportional gain (-)		
k_i	Integral gain (-)		
\dot{m}	Mass flow rate (kg/s)		

Q_{heater}	Auxiliary heat from an electric heater (W)
Re	Reynolds number (-)
skew	Skewness factor (-)
U	Thermal conductance (W/K)
Δh	Enthalpy of fusion (J/kg)
Δt	Simulation time step (second)

REFERENCES

1. Jensen, S.Ø., et al., *IEA EBC Annex 67 energy flexible buildings*. Energy and Buildings, 2017. **155**: p. 25-34.
2. Mao, N., et al., *Numerical investigations on the effects of envelope thermal loads on energy utilization potential and thermal non-uniformity in sleeping environments*. Building and Environment, 2017. **124**: p. 232-244.
3. Mao, N., et al., *A numerical study on influences of building envelope heat gain on operating performances of a bed-based task/ambient air conditioning (TAC) system in energy saving and thermal comfort*. Applied energy, 2017. **192**: p. 213-221.
4. Du, K., et al., *A review of the applications of phase change materials in cooling, heating and power generation in different temperature ranges*. Applied energy, 2018. **220**: p. 242-273.
5. Zhou, Z., et al., *Phase change materials for solar thermal energy storage in residential buildings in cold climate*. Renewable and Sustainable Energy Reviews, 2015. **48**: p. 692-703.
6. Paris, J., M. Falardeau, and C. Villeneuve, *Thermal storage by latent heat: a viable option for energy conservation in buildings*. Energy Sources, 1993. **15**(1): p. 85-93.
7. Soares, N., et al., *Review of passive PCM latent heat thermal energy storage systems towards buildings' energy efficiency*. Energy and buildings, 2013. **59**: p. 82-103.
8. Bourne, S. and A. Novoselac. *Compact PCM-based thermal stores for shifting peak cooling loads*. in *Building Simulation*. 2015. Springer.
9. Yu, Z.J., et al., *Control strategies for integration of thermal energy storage into buildings: State-of-the-art review*. Energy and Buildings, 2015. **106**: p. 203-215.
10. Berardi, U. and S. Soudian. *Benefits of latent thermal energy storage in the retrofit of Canadian high-rise residential buildings*. in *Building Simulation*. 2018. Springer.
11. Pasupathy, A. and R. Velraj, *Effect of double layer phase change material in building roof for year round thermal management*. Energy and Buildings, 2008. **40**(3): p. 193-203.
12. Kuznik, F. and J. Virgone, *Experimental investigation of wallboard containing phase change material: Data for validation of numerical modeling*. Energy and Buildings, 2009. **41**(5): p. 561-570.
13. Dermardiros, V., *Modelling and experimental evaluation of an active thermal energy storage system with phase-change materials for model-based control*. 2015, Concordia University.

14. Papachristou, A.C., et al., *A numerical and experimental study of a simple model-based predictive control strategy in a perimeter zone with phase change material*. Science and Technology for the Built Environment, 2018: p. 1-12.
15. Bastani, A., F. Haghighat, and C.J. Manzano, *Investigating the effect of control strategy on the shift of energy consumption in a building integrated with PCM wallboard*. Energy Procedia, 2015. **78**: p. 2280-2285.
16. Zhu, N., Z. Ma, and S. Wang, *Dynamic characteristics and energy performance of buildings using phase change materials: a review*. Energy Conversion and Management, 2009. **50**(12): p. 3169-3181.
17. Childs, K. and T. Stovall, *Potential energy savings due to phase change material in a building wall assembly: an examination of two climates*. Oak Ridge National Laboratory, Oak Ridge, TN, Technical Report No. ORNL/TM-2012/6, 2012.
18. Bigaila, E. and A. Athienitis, *Modeling and simulation of a photovoltaic/thermal air collector assisting a façade integrated small scale heat pump with radiant PCM panel*. Energy and Buildings, 2017. **149**: p. 298-309.
19. Athienitis, A., et al., *Investigation of the thermal performance of a passive solar test-room with wall latent heat storage*. Building and Environment, 1997. **32**(5): p. 405-410.
20. Farid, M.M., et al., *A review on phase change energy storage: materials and applications*. Energy conversion and management, 2004. **45**(9-10): p. 1597-1615.
21. Soares, N., C.F. Reinhart, and A. Hajiah. *Simulation-based analysis of the use of PCM-wallboards to reduce cooling energy demand and peak-loads in low-rise residential heavyweight buildings in Kuwait*. in *Building Simulation*. 2017. Springer.
22. Nikoofard, S., V.I. Ugursal, and I. Beausoleil-Morrison. *Techno-economic assessment of the impact of phase change material thermal storage on the energy consumption and GHG emissions of the Canadian Housing Stock*. in *Building Simulation*. 2015. Springer.
23. Guarino, F., et al., *PCM thermal storage design in buildings: Experimental studies and applications to solarium in cold climates*. Applied energy, 2017. **185**: p. 95-106.
24. Mosaffa, A., et al., *Thermal performance of a multiple PCM thermal storage unit for free cooling*. Energy Conversion and Management, 2013. **67**: p. 1-7.
25. Morovat, N. and A.K. Athienitis, *Impact of building-integrated PCM on the indoor thermal environment and energy performance of an office zone*, in *12th IIR Conference on Phase-Change Materials and Slurries for Refrigeration and Air Conditioning (PCM 2018)*. 2018: Orford (Québec), Canada. p. 8.
26. Fleischer, A.S., *Fundamental thermal analysis*, in *Thermal Energy Storage Using Phase Change Materials*. 2015, Springer. p. 75-85.
27. Heier, J., C. Bales, and V. Martin, *Combining thermal energy storage with buildings—a review*. Renewable and Sustainable Energy Reviews, 2015. **42**: p. 1305-1325.
28. Hed, G. and R. Bellander, *Mathematical modelling of PCM air heat exchanger*. Energy and Buildings, 2006. **38**(2): p. 82-89.
29. Zalba, B., et al., *Review on thermal energy storage with phase change: materials, heat transfer analysis and applications*. Applied Thermal Engineering, 2003. **23**(3): p. 251-283.
30. DuPont, *DuPont Energain - Energy-saving thermal mass systems*. Available at: http://www.cse.fraunhofer.org/hs-fs/hub/55819/file-14736951-pdf/docs/energain_flyer.pdf 2/15/2019.

31. Dermardiros, V. and A. Athienitis. *Comparison of PCM-active thermal storage systems integrated in building enclosures*. in *10th Conference on Advanced Building Skins*. 2015.
32. Afroz, Z., et al., *Modeling techniques used in building HVAC control systems: A review*. Renewable and Sustainable Energy Reviews, 2017.
33. Tabares-Velasco, P., C. Christensen, and M. Bianchi, *Simulated Peak Reduction and Energy Savings of Residential Building Envelope With Phase Change Materials*. ASHRAE Trans, 2012. **118**(2): p. 90-97.
34. Le Dréau, J. and P. Heiselberg, *Energy flexibility of residential buildings using short term heat storage in the thermal mass*. Energy, 2016. **111**: p. 991-1002.
35. Reynders, G., et al., *Energy flexible buildings: An evaluation of definitions and quantification methodologies applied to thermal storage*. Energy and Buildings, 2018.
36. Barzin, R., et al., *Application of weather forecast in conjunction with price-based method for PCM solar passive buildings—An experimental study*. Applied Energy, 2016. **163**: p. 9-18.
37. Crawley, D.B., et al., *Energy plus: energy simulation program*. ASHRAE journal, 2000. **42**(4): p. 49-56.
38. Manning, M., et al., *The Effects of Thermostat Setting on Seasonal Energy Consumption at the CCHT Research Facility*. CCHT Report, 2005.
39. Moon, J.W. and S.-H. Han, *Thermostat strategies impact on energy consumption in residential buildings*. Energy and Buildings, 2011. **43**(2-3): p. 338-346.
40. Candanedo, J.A., et al., *Near-optimal transition between temperature setpoints for peak load reduction in small buildings*. Energy and Buildings, 2015. **87**: p. 123-133.
41. Braun, J.E. and K.-H. Lee, *An Experimental Evaluation of Demand Limiting Using Building Thermal Mass in a Small Commercial Building*. ASHRAE transactions, 2006. **112**(1).
42. Lee, K.-h. and J.E. Braun, *Model-based demand-limiting control of building thermal mass*. Building and Environment, 2008. **43**(10): p. 1633-1646.
43. D'Angiolella, R., M. de Groot, and M. Fabbri, *NZEB 2.0: Interactive players in an evolving energy system*. REHVA J, 2016. **53**: p. 52-55.
44. De Coninck, R. and L. Helsens, *Bottom-up quantification of the flexibility potential of buildings*, in: *Building Simulation*. 13th International Conference of the International Building Performance Simulation Association, IBPSA, Aix-les-Bains, France, 2013.